ADVANCED MATERIALS
www.advmat.de

Nanoscale Distortions of Si Quantum Wells in Si/SiGe Quantum-Electronic Heterostructures

P. G. Evans, D. E. Savage, J. R. Prance, C. B. Simmons, M. G. Lagally, S. N. Coppersmith, M. A. Eriksson, and T. U. Schülli*

Devices exploiting individual quantum states of electrons promise to extend dramatically the capabilities of silicon integrated electronics. One route to forming such devices is via coupled electrostatically defined quantum dots in which electrons are confined in a thin strained Si layer on SiGe.[1,2] The unique advantage of forming such quantum dots in Si is the long quantum dephasing time afforded by the lack of a nuclear spin in ^{28}Si.[3–5] It is proving challenging to build on this promise because there are significant variations in the properties of individual devices fabricated in the Si/SiGe system. The SiGe substrate in fact introduces this problem: randomness in plastic relaxation during its growth imprints a complex structural state on the silicon quantum well (QW).[6] Structural issues are relevant because the morphology of the QW interfaces affects the sub-bands of the QW[7,8] and single-particle states within quantum dots.[9,10] The length scales, magnitudes, and structural motifs of the distortions have remained unknown, and as a result it has not been possible to optimize quantum device structures to mitigate structural inhomogeneity. Here we show using X-ray nanodiffraction that there are significant interface structure variations within Si QWs, that these variations are sufficient to alter the properties of quantum-information devices, and that the design of such devices must account for these effects.

The present understanding of nanostructural effects on the quantum-mechanical properties of Si/SiGe and related heterostructures is based on a variety of largely indirect probes. Structural influences on transport in epitaxially grown Si or GaAs-based quantum-electronic materials have in earlier work been characterized by combined electronic-transport and atomic-force microscopy measurements,[11,12] by varying the size and positions of quantum dots,[13–16] by Raman scattering,[17] and through the introduction of deliberate surface patterns.[18] None of these previous approaches provide the direct information on crystallographic structure and defects required to understand the role of specific structural features. In particular, the critical issue of differences in the interface structure over lateral distances on the order of the size of the quantum dots has not yet been addressed. Although such information is in principle available via modern methods of X-ray scattering, prior spatially resolved X-ray measurements on the Si/SiGe heterostructure system have in general focused on the SiGe layers rather than the Si QW.[19,20] We thus know much about the surfaces, substrates, and electronic properties of the material surrounding the QW, but comparatively little about the Si QW itself, especially its strain, orientation, and interfacial roughness at the 100 nm lateral length scale relevant to quantum-dot devices. Recent advances in X-ray nanodiffraction experimental methods now allow the QW to be studied directly at the relevant spatial scale in samples identical to those used in electrical studies. We find that the crystallographic orientation of the nominally (001) oriented Si QW layer varies sufficiently over distances of 0.5 to 1 μm to be of concern for electron spin qubits. We also find variations in the intensity of the diffracted X-rays that are consistent with atomic-layer-scale variation in the thickness of the QW layer at shorter, 100 nm, length scales.

The experimental arrangement of the synchrotron X-ray nanodiffraction study is shown in **Figure 1**a. X-rays from an undulator insertion device at beamline ID01 of the European Synchrotron Radiation Facility with a photon energy of 10 keV were focused using a 200 μm-diameter Fresnel zone plate to a spot size of approximately 150 nm on the sample. Unfocused X-rays were spatially filtered using an order sorting aperture. The sample was mounted on the center of an X-ray diffractometer, which provided the motions necessary to rotate the sample with respect to the incident beam. The location of the beam on the sample was varied using a piezoelectric translation stage. The working distance of the X-ray focusing optics was sufficiently large to allow the heterostructure to be characterized without removing it from the electrical measurement circuit, as in Figure 1a. Diffracted X-rays were detected using a pixel array detector, which provided images of the X-ray intensity on a 2° × 2° segment of the Ewald sphere. Three-dimensional diffraction patterns were recorded by acquiring a series of two-dimensional detector images at different orientations of the sample with respect to the incident beam and reconstructing a three-dimensional rendering of the distribution of intensity in reciprocal space. The Fresnel zone plate focusing optics introduced a beam divergence of approximately 0.05°, which is significantly less than the natural angular widths of the diffraction features associated with layers within the SiGe/Si heterostructure. The divergence of the beam introduced by focusing thus had a minimal impact on the interpretation of the X-ray nanodiffraction experiments.

Prof. P. G. Evans, Dr. D. E. Savage, Dr. J. R. Prance, Dr. C. B. Simmons, Prof. M. G. Lagally, Prof. S. N. Coppersmith, Prof. M. A. Eriksson
University of Wisconsin
Madison, WI 53706, USA
E-mail: evans@engr.wisc.edu
Dr. T. U. Schülli
European Synchrotron Radiation Facility
Grenoble, 38000 France

DOI: 10.1002/adma.201201833

© 2012 WILEY-VCH Verlag GmbH & Co. KGaA, Weinheim

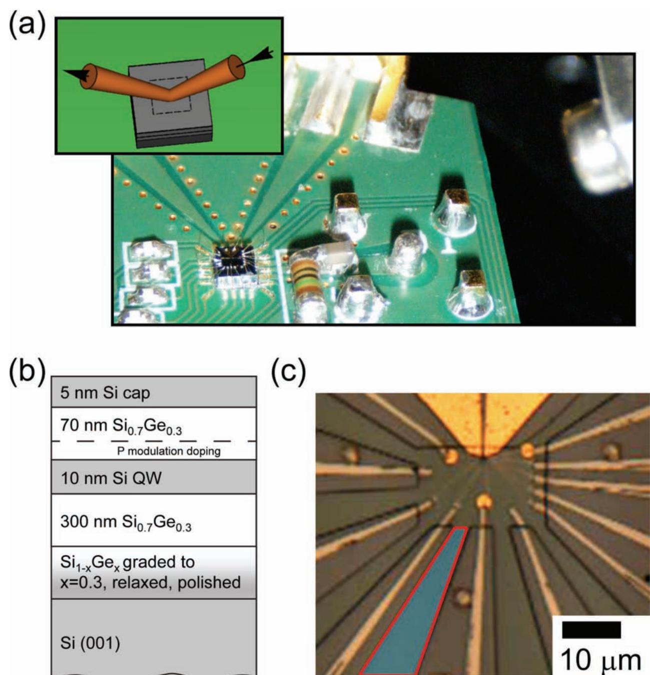

Figure 1. X-ray nanodiffraction characterization of a Si QW. a) Synchrotron X-ray study of a Si quantum device fully integrated in a measurement circuit. The Si/SiGe heterostructure is located on the Si (001) crystal at the lower left of the photograph. A diagram of the focused X-ray beam is inset. b) Layer sequence of the Si/SiGe heterostructure. c) Optical micrograph of the lithographically patterned Si QW. The X-ray study is conducted within an area of unprocessed Si/SiGe extending radially from the quantum dot at the center of the image. One such area is highlighted by the shaded region.

The Si/SiGe heterostructure of interest is grown on a SiGe (001) substrate, which is the top layer of a multilayer in which the Ge concentration is linearly graded to 30% over a thickness of several μm, starting from pure Si (001) (Figure 1b). The substrate surface is polished to remove the variation in the height of the surface that accompanies average plastic relaxation.[21,22] The Si QW is grown pseudomorphically on this substrate, with the following sequence of layers: 300 nm $Si_{0.7}Ge_{0.3}$, the 10 nm strained-Si QW, 23 nm $Si_{0.7}Ge_{0.3}$, 2 nm P-doped $Si_{0.7}Ge_{0.3}$ to provide modulation doping, 45 nm $Si_{0.7}Ge_{0.3}$, and a 5 nm Si cap. The growth sequence creates a nominal biaxial strain of 1% in the Si QW, but, more importantly, leads to variations in strain and orientation in the Si QW because of the spatial distribution of defects associated with the plastic relaxation of the SiGe. The SiGe is thus only an approximation of the ideal substrate for the subsequent Si QW. The Si QW layer was probed in a heterostructure on which an electrostatically defined submicron Si quantum dot had been created, but in an area away from the contacts defining the QD. A number of large unpatterned areas of the Si QW are found near the quantum dot, exemplified by the shaded region in Figure 1c. We use one of these for the measurements.

A diagram of the three-dimensional reciprocal space of the Si/SiGe heterostructure in the region near the Si (004) Bragg reflection is shown in **Figure 2**a. SiGe layers produce a broad distribution of intensity along the angular axes labeled tilt and $\Delta 2\theta$ in Figure 2a, arising from the gradient in Ge composition and from the crystallographic tilt induced during plastic strain relaxation. The smoothness and thinness of the Si QW layer lead to an additional rod of intensity extending along the direction normal to the interfaces of the QW, approximately along the vertical direction of Figure 2a. The large thickness of the SiGe layers causes diffraction from SiGe to be more tightly confined in the reciprocal-space direction along the surface normal than is the diffraction from the Si QW along its reciprocal-lattice rod. Thus the intensity associated with the Si QW can be straightforwardly distinguished from the far thicker SiGe layers. The ease of distinguishing the Si QW from the SiGe is

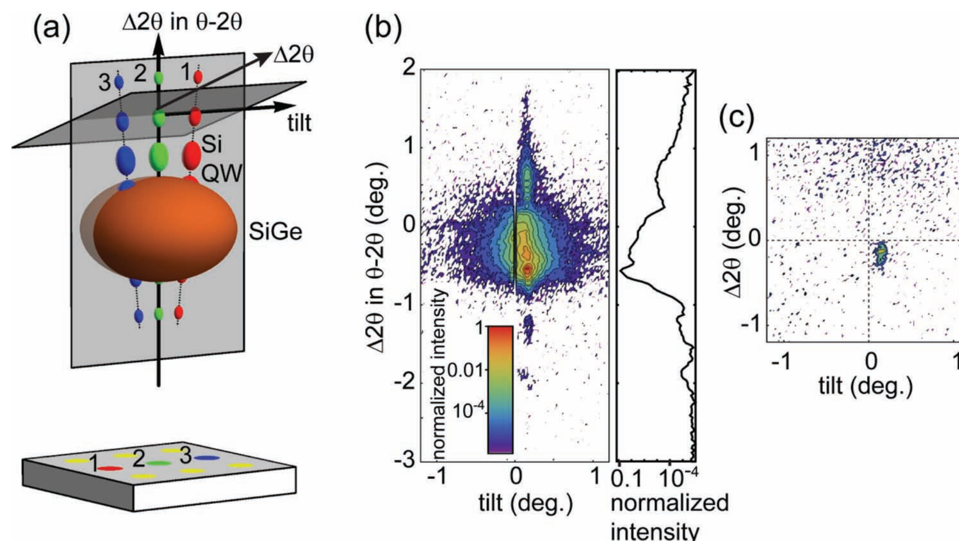

Figure 2. Nanodiffraction patterns. a) Diagram of the three-dimensional reciprocal-space volume near the Si (004) Bragg reflection, with the diffraction signatures of SiGe (large ellipsoid) and of the Si QW at three locations on the surface (1, 2, and 3) in which the crystallographic lattice of the Si QW has slightly different orientations. The vertical and nearly horizontal planes indicate the orientations of the two-dimensional sections shown in b) and c), respectively. b) Two-dimensional section of reciprocal space with a distribution of intensity from SiGe that is broad along the tilt angular axis, and a rod of intensity from the Si QW extending along the vertical direction. The vertical line of reduced intensity is an artifact caused by the pixel-array detector. c) A single diffraction image illustrating the angular displacement of the rod of scattering arising from the Si QW.

© 2012 WILEY-VCH Verlag GmbH & Co. KGaA, Weinheim

useful because it allows the real-space mapping of the QW to be done rapidly and unambiguously. The effect of the variation of the orientation of the crystallographic planes of the QW layer on the three-dimensional diffraction pattern is illustrated in Figure 2a for one particular hypothetical set of misorientations of the Si QW at three locations of the beam on the sample. The misorientations of the Si QW illustrated in Figure 2a lead to a rotation of the diffraction pattern in reciprocal space, which in this example falls along the angular axis labeled tilt.

Two different two-dimensional slices extracted from the experimental three-dimensional reconstruction of reciprocal space are shown in Figure 2b and c. The diffraction data shown in Figure 2b and c were acquired with the beam incident on a single location on the sample and thus provide detailed structural information about that location. The orientations of these slices are shown as the shaded planes in the illustration in Figure 2a. The axes of Figure 2b are chosen to be identical to a conventional reciprocal-space map. The reciprocal-space map diffraction pattern in Figure 2b exhibits features arising from SiGe and the Si QW and shows that diffracted X-rays from each layer can be readily distinguished.

Figure 2c is a slice of reciprocal space that is nearly orthogonal to the slice shown in Figure 2b, exhibiting an intense diffraction feature that arises only from the Si QW. The slice in Figure 2c is particularly useful in an experimental sense because it corresponds to a single detector image and can thus be acquired rapidly as the beam is scanned across the sample. The reciprocal-space location and orientation of the plane of the detector of Figure 2c are such that the rod arising from the Si QW intersects it in one point, visible as the intensity maximum in Figure 2c. Maps of the tilt and other structural parameters of the QW can be determined using the angular shift of this intersection and the intensity of the diffraction at this point. Through this use of the angular position of the maximum intensity in a series of diffraction patterns, the tilt maps can be assembled from a series of single diffraction patterns without varying the angle of incidence of the X-ray beam, thus simplifying the assembly of precise real-space maps by eliminating artifacts associated with the inevitable movement of the X-ray beam along the surface when the sample is rotated. The rod of intensity from the Si QW was acquired with sufficiently high precision that the resolution of the measurement of the center of the diffracted beam was smaller than the divergence of the incident beam. The angular resolution of the results presented in Figure 2c, and hence the resolution of the measurement of the tilt in the Si QW tilt measurement, is better than 0.001°, equivalent to 1–2% of the divergence of the incident X-ray beam.

The relationship between the tilt of the lattice planes within the Si QW and the angular displacement of the diffraction spot is different along the two axes of Figure 2c. In the tilt axis, the misorientation of the lattice planes is a factor of $k/q_{004} \approx 1.09$ greater than the angular displacement of the feature arising from the Si QW.[23] Here k and q_{004} are the magnitudes of wavevectors of the incident beam and the Si (004) reflection, respectively. Along the $\Delta 2\theta$ axis, the angular displacement of the intersection of the rod with the diffraction pattern is twice the angular rotation of the lattice.

The orientation of the crystallographic planes within the Si QW can vary even though the growth of the QW occurs on a SiGe substrate in which the average strain resulting from the growth of SiGe on bulk Si (001) has been plastically relaxed. The dislocations produced during the relaxation process lead to a non-uniform distribution of crystallographic orientations and results in localized strain gradients. In this Si/SiGe heterostructure, the topographic cross hatch characteristic of the relaxation in strain-graded SiGe has been removed by polishing. Polishing away the roughness (i.e., the cross hatch) created by dislocation formation and relaxation in the step graded growth does not remove the distribution of mosaic blocks that is created via plastic relaxation, nor does it remove the dislocation pileups that lead to non-uniform strain in the relaxed SiGe layer on which the Si QW is grown. The geometric arrangement of the interfaces and the planes within them are shown in a schematic cross section of the Si QW in **Figure 3**a.

Figure 3b and c show the magnitude and direction of differences between the local orientation of the Si QW layer and its average orientation within one of the unprocessed areas of Figure 1c. The angular displacements within the 5 μm × 5 μm area of Figure 3b and c are as large as 0.022°, varying over lateral distances of approximately 1 μm and exhibiting larger areas in which the direction of the tilt is relatively constant. The crystallographic distortion shown in Figure 3 factors significantly into the strain distribution in the QW. The orientation gradients correspond to a radius of curvature of 3 mm, or a difference in strain of 3×10^{-7} across the 10 nm thickness of the quantum well. Regions of opposite curvature thus differ in strain by approximately 10^{-6}.

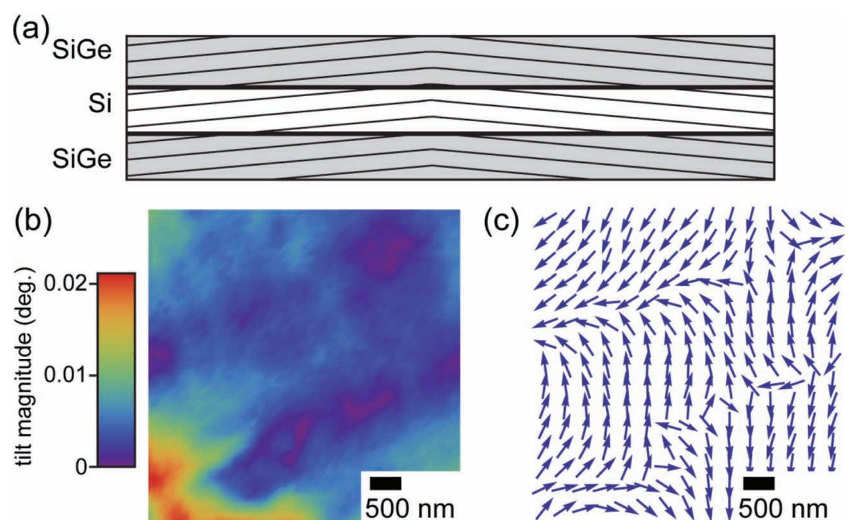

Figure 3. Crystallographic tilts within the Si QW. a) Illustration of the persistence of misorientation in the silicon planes despite the planarization of the surface of the SiGe buffer. Maps of b) magnitude and c) direction crystallographic planes in the QW relative to the average orientation.

© 2012 WILEY-VCH Verlag GmbH & Co. KGaA, Weinheim

Strain variations due to the curvature of the crystallographic planes of the Si QW drastically modify the energy levels of electron sub-bands in the QW, and, by extension, in electrostatically defined quantum dots that are subsequently created within the QWs. The localized curvature of the crystallographic planes within the Si QW produces a strain that is superimposed on the larger nominal lattice-mismatch induced biaxial strain imposed by the $Si_{0.70}Ge_{0.30}$ substrate. For a QW grown on a fully plastically relaxed $Si_{0.7}Ge_{0.3}$ substrate, this change in local strain corresponds to a local change in the conduction band energy of 0.014 meV or 165 mK.[1] The electron temperature in electron spin qubits in electrostatically defined Si quantum dots is in fact only slightly lower than the energy shifts induced by this curvature.[24] Electronic variations with the order of magnitude we have found thus have the potential to be extremely important contributors to the low-temperature electronic energy landscape and must be precisely controlled.

Further nanoscale structural information can be obtained by examining the intensity of the diffracted X-ray beam. **Figure 4**a shows a map of the intensity of the Si QW diffraction signal within the area of the sample surface spanned by the maps in Figure 3. The intensity varies by approximately 20% across the full extent of the image. The tilts of the QW layer are uncorrelated with the variation in Figure 4a and are not sufficient to produce intensity changes of this magnitude. One possible mechanism leading to a change in the diffracted intensity would be a rotation of the Si QW to an orientation at which the diffracted intensity along the Si QW rod is zero. The tilt required to do this would have a magnitude of half of the angular separation of adjacent QW thickness fringes, $\frac{\pi}{\sqrt{k^2-q_{004}^2}}$, approximately 0.4° for thickness t = 10 nm. With the observed maximum orientation variation of 0.02°, the expected intensity variation due to tilt is 1%. At smaller lateral distances the tilt observed in Figure 3b is much less, and we thus conclude that the role of tilt in varying the intensity is negligible.

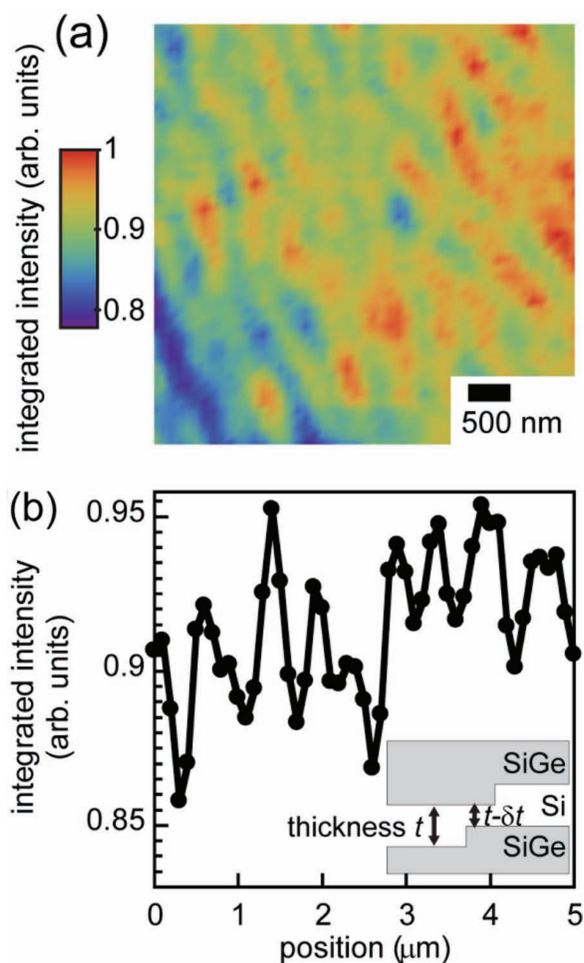

Figure 4. Nanoscale thickness variation. a) Map of the normalized intensity of the Si QW diffraction signature in the same region of the sample surface as shown Figure 2. b) Variation of the intensity along a horizontal line near the top of the image. The inset shows how decorrelation of atomic steps during epitaxy can lead to local thickness variations.

A more likely origin of the intensity variation shown in Figure 4 lies in local variations of the thickness of the Si QW layer. A thickness change of magnitude δt would lead to a fractional change in intensity $(\delta t/t)^2$. The experimentally observed intensity in the single scan line shown in Figure 4b varies by approximately 5% over 100 nm-scale distances, requiring $\delta t/t \approx$ 2%. For a QW with t = 10 nm such a thickness variation corresponds to only a few atomic layers, which can easily arise in epitaxy.[25,26] Thickness changes of 1–2 layers can arise simply from the decorrelation of steps on the top and bottom surfaces of the QW, as illustrated in the inset of Figure 4b. It is precisely at this atomic scale that the detailed arrangement of steps at the top QW interface is predicted to affect interference between the individual quantum states of nearly degenerate conduction band valleys.[9,27,28]

Beyond the crystallographic distortion and thickness variation intrinsic to the Si QW/plastically relaxed SiGe system that we have reported here, we expect that additional electronic effects will arise from the processing required to produce quantum dots within the QW. For example, metallizations can produce strains of up to 0.1%, falling off over distances as large as 1–2 μm from the edges of electrodes.[29] Strain gradients of this magnitude would modify the energy of electronic states in quantum dots to an even greater extent than we have already found. As the technology associated with quantum-information advances (e.g., via the formation of qubits in specifically grown nanostructures),[30] such structural distortions are likely to play an increasingly large role in influencing quantum transport. The results presented here show that such distortions are an intrinsic part of Si QW systems on plastically relaxed SiGe substrates. Advanced X-ray methods, building from this non-destructive approach, will be particularly valuable in developing strategies to limit deleterious structural effects because characterization can now be conducted with little or no alteration of the QW during sample preparation.

Acknowledgements

Fabrication of Si QW samples was supported by ARO and LPS (W911NF-08-1-0482). This research used NSF-supported shared facilities at the University of Wisconsin-Madison. P.E. gratefully acknowledges support from the ESRF during an extended visit in 2010–2011, and from the

© 2012 WILEY-VCH Verlag GmbH & Co. KGaA, Weinheim

US Department of Energy, Office of Basic Energy Sciences, Division of Materials Sciences and Engineering under award DE-FG02-10ER46147 for the development of data-analysis techniques.

Received: May 7, 2012
Published online: July 16, 2012

[1] F. Schaffler, *Semicond. Sci. Technol.* **1997**, *12*, 1515.
[2] M. Friesen, P. Rugheimer, D. E. Savage, M. G. Lagally, D. W. van der Weide, R. Joynt, M. A. Eriksson, *Phys. Rev. B: Condens. Matter* **2003**, *67*, 121301.
[3] A. Morello, J. J. Pla, F. A. Zwanenburg, K. W. Chan, K. Y. Tan, H. Huebl, M. Mottonen, C. D. Nugroho, C. Y. Yang, J. A. van Donkelaar, A. D. C. Alves, D. N. Jamieson, C. C. Escott, L. C. L. Hollenberg, R. G. Clark, A. S. Dzurak, *Nature* **2010**, *467*, 687.
[4] J. J. L. Morton, D. R. McCamey, M. A. Eriksson, S. A. Lyon, *Nature* **2011**, *479*, 345.
[5] B. M. Maune, M. G. Borselli, B. Huang, T. D. Ladd, P. W. Deelman, K. S. Holabird, A. A. Kiselev, I. Alvarado-Rodriguez, R. S. Ross, A. E. Schmitz, M. Sokolich, C. A. Watson, M. F. Gyure, A. T. Hunter, *Nature* **2012**, *481*, 344.
[6] P. M. Mooney, J. O. Chu, *Annu. Rev. Mater. Sci.* **2000**, *30*, 335.
[7] S. Goswami, K. A. Slinker, M. Friesen, L. M. McGuire, J. L. Truitt, C. Tahan, L. J. Klein, J. O. Chu, P. M. Mooney, D. W. van der Weide, R. Joynt, S. N. Coppersmith, M. A. Eriksson, *Nature Phys.* **2007**, *3*, 41.
[8] M. Friesen, M. A. Eriksson, S. N. Coppersmith, *Appl. Phys. Lett.* **2006**, *89*, 202106.
[9] M. Friesen, S. N. Coppersmith, *Phys. Rev. B: Condens. Matter* **2010**, *81*, 115324.
[10] M. G. Borselli, R. S. Ross, A. A. Kiselev, E. T. Croke, K. S. Holabird, P. W. Deelman, L. D. Warren, I. Alvarado-Rodriguez, I. Milosavljevic, F. C. Ku, W. S. Wong, A. E. Schmitz, M. Sokolich, M. F. Gyure, A. T. Hunter, *Appl. Phys. Lett.* **2011**, *98*, 123118.
[11] R. L. Willett, J. W. P. Hsu, D. Natelson, K. W. West, L. N. Pfeiffer, *Phys. Rev. Lett.* **2001**, *87*, 126803.
[12] R. M. Feenstra, M. A. Lutz, F. Stern, K. Ismail, P. M. Mooney, F. K. Legoues, C. Stanis, J. O. Chu, B. S. Meyerson, *J. Vac. Sci. Technol. B* **1995**, *13*, 1608.
[13] I. H. Chan, R. M. Clarke, C. M. Marcus, K. Campman, A. C. Gossard, *Phys. Rev. Lett.* **1995**, *74*, 3876.
[14] J. A. Folk, S. R. Patel, S. F. Godijn, A. G. Huibers, S. M. Cronenwett, C. M. Marcus, K. Campman, A. C. Gossard, *Phys. Rev. Lett.* **1996**, *76*, 1699.
[15] S. Amasha, K. MacLean, I. P. Radu, D. M. Zumbuehl, M. A. Kastner, M. P. Hanson, A. C. Gossard, *Phys. Rev. Lett.* **2008**, *100*, 046803.
[16] Z. Shi, C. B. Simmons, J. R. Prance, J. K. Gamble, M. Friesen, D. E. Savage, M. G. Lagally, S. N. Coppersmith, M. A. Eriksson, *Appl. Phys. Lett.* **2011**, *99*, 233108.
[17] J. M. Hartmann, A. Abbadie, D. Rouchon, M. Mermoux, T. Billon, *Semicond. Sci. Technol.* **2007**, *22*, 362.
[18] D. Kamburov, H. Shapourian, M. Shayegan, L. N. Pfeiffer, K. W. West, K. W. Baldwin, R. Winkler, *Phys. Rev. B: Condens. Matter* **2012**, *85*, 121305.
[19] D. E. Eastman, C. B. Stagarescu, G. Xu, P. M. Mooney, J. L. Jordan-Sweet, B. Lai, Z. Cai, *Phys. Rev. Lett.* **2002**, *88*, 156101.
[20] S. Mochizuki, A. Sakai, N. Taoka, O. Nakatsuka, S. Takeda, S. Kimura, M. Ogawa, S. Zaima, *Thin Solid Films* **2006**, *508*, 128.
[21] The polished SiGe/Si substrates used in this work were supplied by IQE, Inc., Cardiff, UK.
[22] K. Sawano, S. Koh, Y. Shiraki, Y. Hirose, T. Hattori, K. Nakagawa, *Appl. Phys. Lett.* **2003**, *82*, 412.
[23] P. G. Evans, P. P. Rugheimer, M. G. Lagally, C. H. Lee, A. Lal, Y. Xiao, B. Lai, Z. Cai, *J. Appl. Phys.* **2005**, *97*, 103501.
[24] C. B. Simmons, J. R. Prance, B. J. Van Bael, T. S. Koh, Z. Shi, D. E. Savage, M. G. Lagally, R. Joynt, M. Friesen, S. N. Coppersmith, M. A. Eriksson, *Phys. Rev. Lett.* **2011**, *106*, 156804.
[25] C. Teichert, *Phys. Rep.* **2002**, *365*, 335.
[26] J. Tersoff, Y. H. Phang, Z. Y. Zhang, M. G. Lagally, *Phys. Rev. Lett.* **1995**, *75*, 2730.
[27] M. Friesen, S. Chutia, C. Tahan, S. N. Coppersmith, *Phys. Rev. B: Condens. Matter* **2007**, *75*, 115318.
[28] L. M. McGuire, M. Friesen, K. A. Slinker, S. N. Coppersmith, M. A. Eriksson, *New J. Phys.* **2010**, *12*, 033039.
[29] C. E. Murray, K. L. Saenger, O. Kalenci, S. M. Polvino, I. C. Noyan, B. Lai, Z. Cai, *J. Appl. Phys.* **2008**, *104*, 013530.
[30] Y. Hu, F. Kuemmeth, C. M. Lieber, C. M. Marcus, *Nature Nanotechnol.* **2012**, *7*, 47.

© 2012 WILEY-VCH Verlag GmbH & Co. KGaA, Weinheim